



# Selective formation of ordered arrays of octacalcium phosphate ribbons on TiO<sub>2</sub> nanotube surface by template-assisted electrodeposition

Yuekun Lai<sup>a,b</sup>, Yongxia Huang<sup>a</sup>, Hui Wang<sup>a</sup>, Jianying Huang<sup>c</sup>, Zhong Chen<sup>b</sup>, Changjian Lin<sup>a,\*</sup>

<sup>a</sup> State Key Laboratory of Physical Chemistry of Solid Surfaces, and College of Chemistry and Chemical Engineering, Xiamen University, Xiamen 361005, China

<sup>b</sup> School of Materials Science and Engineering, Nanyang Technological University, 50 Nanyang Avenue, Singapore 639798, Singapore

<sup>c</sup> Fujian Institute of Research on the Structure of Matter, Chinese Academy of Sciences, Fuzhou 350002, China

## ARTICLE INFO

### Article history:

Received 21 August 2009

Received in revised form 5 October 2009

Accepted 13 October 2009

Available online 23 October 2009

### Keywords:

TiO<sub>2</sub> nanotube

Superhydrophilic–superhydrophobic

Micropatterned template

Electrochemical deposition

Octacalcium phosphate (OCP)

## ABSTRACT

Using a patterned superhydrophobicity/superhydrophilicity template, micropatterned octacalcium phosphate (OCP) has been successfully fabricated on TiO<sub>2</sub> nanotube array surface. The resultant OCP micropattern has been characterized with scanning electron microscopy, optical microscopy, X-ray diffraction and electron probe microanalyzer. It is shown that the ribbon-like OCP crystals possess a highly ordered and hierarchically porous structure at nano–micro-scales. They can be selectively grown at superhydrophilic areas which are confined by the hydrophobic regions. The high wetting contrast template proves to be useful for constructing well-defined dual scale OCP film with porous structure biomimic to natural bone. A mechanism has been proposed to explain the formation of the OCP patterned film with hierarchically porous structure and distinct selectivity.

© 2009 Elsevier B.V. All rights reserved.

## 1. Introduction

Wettability is an important property of solid substrates that is governed by the chemical composition and geometrical structure [1–5]. Two extremely cases, superhydrophilicity and superhydrophobicity with a water contact angle (CA) below 5° and above 150° respectively, have attracted much interest due to their importance in both fundamental research and practical applications [6–9]. Generally, conventional wettability contrast (hydrophilicity vs. hydrophobicity) at microscopic scale can be achieved on smooth surface by soft lithography [10], or e-beam decomposition self-assembled monolayers (SAMs) [11], direct writing by atomic force microscopy [12], or UV photocatalytic lithography [13]. Among these techniques, photocatalytic lithography is one of the most facile techniques due to its large scale pattern transferability at one single exposure. Recently, some groups have reported the fabrication of surfaces with reversible switching wettability between superhydrophilicity and superhydrophobicity [14–18]. However, the report on the preparation and practical application of superhydrophilic–superhydrophobic surface patterns is still rare [19–22].

The accurately defined surface structure of biomaterials is recognized as a main strategy in the design of the new generation

of bone implants and tissue engineering scaffolds. Many efforts had been made to further improve the bioactivity and biocompatibility for the Ti based materials. Such treatments include surface coating of calcium phosphate (CaP) bioactive layers or chemical modifications to enhance hydroxyapatite formation. Octacalcium phosphate (Ca<sub>8</sub>H<sub>2</sub>(PO<sub>4</sub>)<sub>6</sub>·5H<sub>2</sub>O, OCP) was recognized as an important precursor phase that can spontaneously convert to biological apatite [23,24]. It is well known that the biological properties of the biomaterials depend not only on its chemical compositions, but also the biomimic structures. OCP coating comprised of novel nano–micro-dual scale structures is biomimic to natural bone and is favorable for cell anchoring and cell culture due to its run-through structure. However, little work has been done on the fabrication of bioactive OCP nano–micro-dual scale patterning films. Potential applications of biomaterials patterning may include biochips, antibodies, cells and other sensor arrays [25–28].

In this work, we developed a simple technique to fabricate micro–nano-dual level structured OCP film on bioactive TiO<sub>2</sub> nanotube surfaces with the assistance of superhydrophilic–superhydrophobic patterned template. The effect of the deposition time on morphologies and sizes of OCP had been investigated. Experimental results indicated that the wettability pattern had a great effect on the micro–nano-porous OCP films. This simple method on the fabrication of hierarchically structured film may be conveniently applied to other biomimic functional materials.

\* Corresponding author. Tel.: +86 592 2189354; fax: +86 592 2189354.

E-mail address: [cjlin@xmu.edu.cn](mailto:cjlin@xmu.edu.cn) (C. Lin).

## 2. Experimental

### 2.1. Preparation of superhydrophobic TiO<sub>2</sub> nanotube film

TiO<sub>2</sub> nanotube array film was fabricated by electrochemical anodization of titanium sheets (purity 99.5%) in 0.5 wt.% HF electrolyte with Pt counter electrode under 20 V for 20 min [29,30]. The as-prepared amorphous TiO<sub>2</sub> nanotubes were calcinated at 450 °C under ambient condition for 2 h to form anatase phase. To obtain superhydrophobic surface, the annealed samples were further treated with a methanolic solution of hydrolyzed 1 wt.% 1H,1H,2H,2H-perfluorooctyl-triethoxysilane (PTES, Degussa Co., Ltd.) for 1 h and subsequently heated at 140 °C for 1 h.

### 2.2. Fabrication of superhydrophilic–superhydrophobic micropattern

The schematic outline of the procedure to fabricate superhydrophilic–superhydrophobic micropatterns on TiO<sub>2</sub> nanotube array surface is shown in Fig. 1. The superhydrophobic surface was patterned by using a mesh photomask shown in Fig. 1a. The corresponding regions on the surface undergo a decrease in hydrophobicity during the UV irradiation. After irradiation for 30 min, water was dropped on irradiated and non-irradiated regions. It was found that the non-irradiated region still repelled water, while water droplets quickly spread out on the film in the UV-irradiated regions (Fig. 1b). Thus, the irradiated area could be distinguished from the non-irradiated area clearly, and the pattern with extreme wettability was realized. Next, we applied this pattern to induce selected OCP crystals growth with high precision (Fig. 1c).

### 2.3. Electrochemical deposition of OCP micropattern

The superhydrophilic–superhydrophobic micropatterned TiO<sub>2</sub> on titanium sheet was used as a template to selectively deposit OCP crystals on the superhydrophilic regions by electrochemical deposition (ECD). The deposition was carried out in a cell controlled by Autolab PGSTAT30 (Eco Chemie, Holland) electrochemical workstation. The deposition electrolyte contained 0.042 mol/L Ca(NO<sub>3</sub>)<sub>2</sub> and 0.025 mol/L NH<sub>4</sub>H<sub>2</sub>PO<sub>4</sub>. The pH value was adjusted to approximately 4.2 with 0.05 mol/L NaOH solution. The ECD was carried out galvanostatically at a cathodic current of 0.5 mA/cm<sup>2</sup> at 67.5 °C for a certain time [31]. The changes in the cathode voltage with time during deposition were monitored by a PC system. Following the precipitation, the specimen was rinsed with deionized water and dried under ambient conditions.

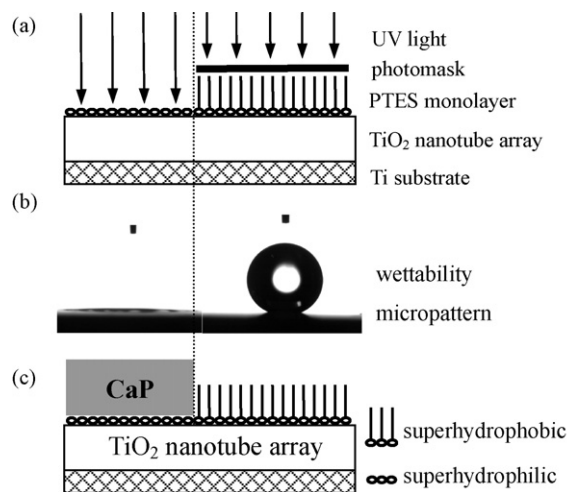


Fig. 1. Schematic outline of the procedures to fabricate nanostructured OCP patterning film by electrochemical deposition based on superhydrophilic–superhydrophobic micropattern.

### 2.4. Morphology and structure characterization

The morphology of the TiO<sub>2</sub> nanotube films and OCP micropatterns were investigated by field-emission scanning electron microscope (FESEM, LEO-1530) and environmental scanning electron microscope (ESEM, Phillips XL-30), respectively. The water CA was measured with an optical contact angle meter system (Dataphysics, OCA-20) at ambient temperature. The experimental data were represented as means ± one standard deviations (SD) for  $n = 5$ . For fluorescence experiments, the obtained patterns were stained with fluorescein sodium, and observed by Karl Zeiss fluorescence microscope (Axioskop2, MAT). The patterned TiO<sub>2</sub> nanotube array samples were observed by optical microscopy (Eclipse E600, Nikon). The chemical element distribution was measured by electron probe microanalyzer (EPMA, JEOL JXA-8100). The crystallinity of the samples was measured using an X-ray diffractometer with Cu K<sub>α</sub> radiation (XRD, Phillips X'pert-PRO PW3040) at 40 kV and 30 mA.

## 3. Results and discussion

### 3.1. Characterization

Fig. 2a shows the top view SEM image of the typical nanostructured TiO<sub>2</sub> film by anodizing Ti sheet under 20 V for 20 min. The surface consists of vertical aligned TiO<sub>2</sub> nanotubes with a single tube diameter of about 80 nm and an average center-to-center

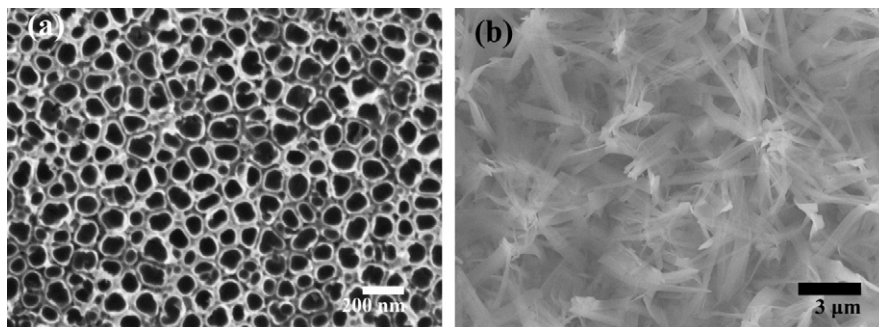
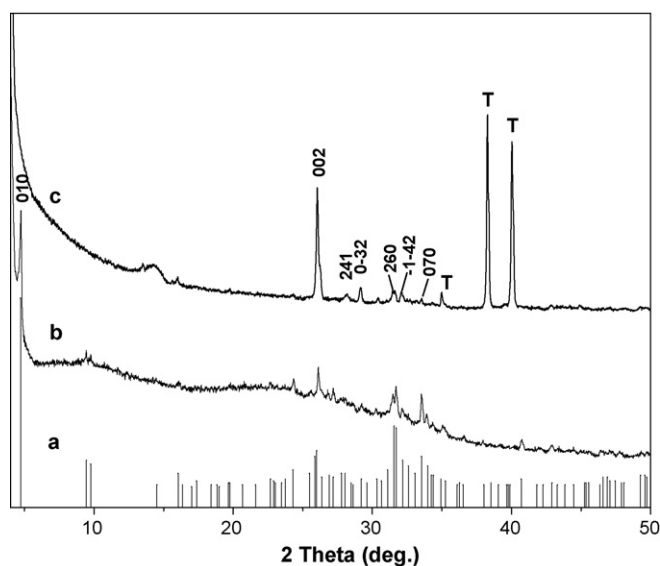


Fig. 2. SEM images of the (a) TiO<sub>2</sub> nanotube array film fabricated by electrochemical anodization; (b) OCP nanostructure layer on TiO<sub>2</sub> nanotube array film by electrochemical deposition for 5 min.



**Fig. 3.** XRD spectra of the OCP thin films selectively deposited onto the patterned  $\text{TiO}_2$  nanotube film by electrochemical deposition. (a) Standard OCP powder spectrum (JCPDS#44-0778); (b) powder scratched from the as-deposited OCP composite film on  $\text{TiO}_2$  nanotube film; (c) the as-deposited OCP composite film (5 min). T represents the titanium substrate.

spacing of 150 nm. Water droplet can quickly spread and wet the as-grown vertically aligned  $\text{TiO}_2$  nanotube array film due to capillary effect caused by the rough tubular structure, indicating such  $\text{TiO}_2$  nanotube array film is superhydrophilic [32–35]. The typical SEM image of OCP composited film on  $\text{TiO}_2$  nanotube array surface by electrochemical deposition for 5 min is shown in Fig. 2b. It can see that quasi-perpendicular ribbon-like crystals of several hundred nanometers in width are uniformly grown on the  $\text{TiO}_2$  nanotube array surface.

Fig. 3a and b shows the XRD spectra of the standard OCP powders (refer to JCPDS#44-0778) and the powders scratched from the as-deposited OCP composite film on the patterned  $\text{TiO}_2$  nanotube film (5 min). T represents the titanium substrate. The spectra of the powders (Fig. 3b), scraped from the coatings, exhibit a typical diffraction peak at  $2\theta = 4.7^\circ$  corresponding to the (100) plane of OCP. The EDS measurement of the as-prepared Ca/P composite layer also shows that the average Ca/P molar ratio is 1.28 (see supporting information Fig. S1 and Table S1), which is close to that of stoichiometric OCP (1.33). The spectrum (curve c) of the OCP thin films selectively deposited onto the  $\text{TiO}_2$  nanotube film by electrochemical deposition shows a strong diffraction peak at  $2\theta = 26.0^\circ$  corresponding to the (002) plane. It indicates that

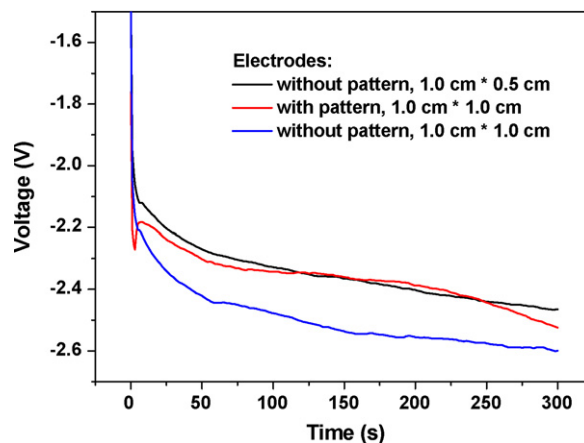


**Fig. 4.** Electrochemical deposition curves of OCP layer on different electrodes.

ribbon-like crystals confined and induced by the template on titanium substrate are preferential along the *c*-axis. This agrees with the observed vertical alignment shown in the SEM graph (Fig. 2b).

### 3.2. Effect of $\text{TiO}_2$ nanotube array on wettability

The roughened  $\text{TiO}_2$  surface was modified with a self-assembly monolayer (SAM) of hydrophobic PTES molecule. The water CA on such rough nanotube film with PTES modification is around  $156 \pm 1.0^\circ$ , indicating that the special nanotube film is superhydrophobic. This effect should allow us to prepare superhydrophobic and superhydrophilic micro-regions on biocompatible Ti substrate. However, the CA of the PTES-modified “flat”  $\text{TiO}_2$  surface (annealed with  $450^\circ\text{C}$  for 1 h) is only  $115.0 \pm 1.2^\circ$  and the CA only decreases to  $26.4 \pm 5.5^\circ$  with an UV-irradiated time of 30 min. Such different contact angle change is due to the different photocatalytic activities of  $\text{TiO}_2$  films. The decomposition rate of the PTES monolayer on the compact  $\text{TiO}_2$  films is lower than that of rough  $\text{TiO}_2$  nanotube films. Moreover, the amplified effect of the rough  $\text{TiO}_2$  nanotube array surface has a great influence on the rapid change of the contact angle. This result is similar to that reported by Zhu et al. [36]. It is interesting to note that the UV-irradiated sample shows hydrophobic character once again when it is coated with the PTES. Therefore, by alternating SAM and UV irradiation, the superhydrophobicity and superhydrophilicity on the rough nanotube surfaces can be reversibly switched. Compared with the unobvious disparity (only around  $90^\circ$ ) on a smooth surface, the wettability contrast on the rough  $\text{TiO}_2$  nanotube surface is more than  $150^\circ$ .

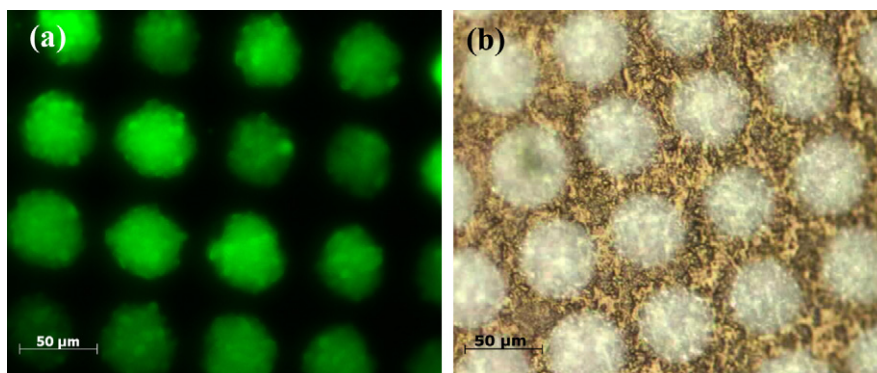
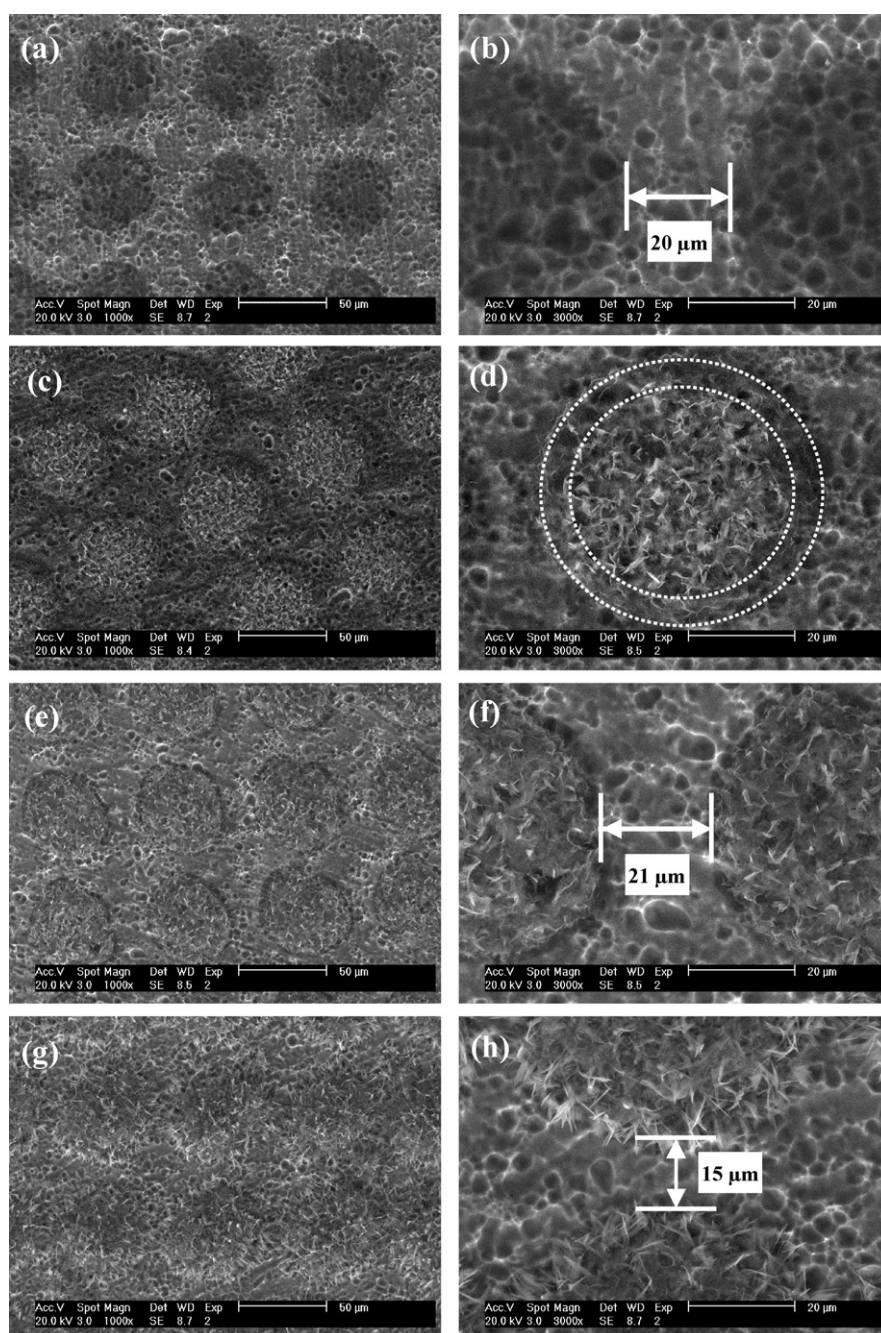


**Fig. 5.** Optical micrographs of the superhydrophilic-superhydrophobic template and patterned OCP thin films selectively deposited in predefined superhydrophilic regions by electrochemical deposition for 5 min: (a) fluorescence pattern and (b) OCP pattern.

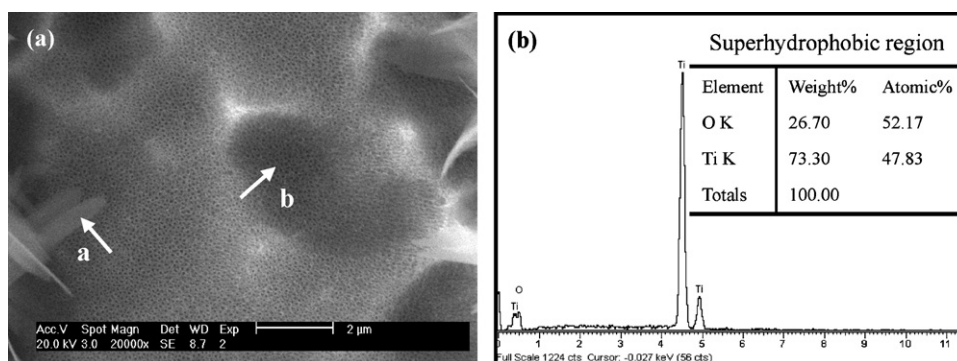
### 3.3. OCP micropattern characterization

Fig. 4 shows the changes of the electrochemical deposition cathode potential with the time under a constant current density ( $0.5 \text{ mA/cm}^2$ ). It is clear that the cathode potential jumps immediately at the initial moment and continuously moves toward the negative values throughout the ECD process. The patterned electrode with exposed area of  $1.0 \text{ cm} \times 1.0 \text{ cm}$  exhibits obvious lower negative voltage than that of the electrode without pattern under identical conditions. However, it shows nearly the similar negative voltage on the electrode with area of  $1.0 \text{ cm} \times 0.5 \text{ cm}$ . This is because that half of the area of the patterned electrode is superhydrophobic, which reduces the effective working area to some extent during the electrochemical deposition process.

Fig. 5a shows a typical fluorescence microscopic image of superhydrophilic–superhydrophobic micropattern on  $\text{TiO}_2$  nanotube surface. As can be seen, the green dots ( $\sim 50 \mu\text{m}$  in diameter and  $\sim 20 \mu\text{m}$  spacing) are clearly imaged through the fluorescence contrast between the UV-irradiated superhydrophilic and masked superhydrophobic regions. The photo-irradiated dots exhibit a uniformly stronger fluorescence against the surrounding dark background due to the high affinity of the fluorescent probes to the superhydrophilic regions. Therefore, a clearly well-defined fluorescence pattern based on the superhydrophilic–superhydrophobic pattern is obtained. Fig. 5b displays the identical patterning of OCP biomaterials deposited on the superhydrophilic–superhydrophobic patterns on  $\text{TiO}_2$  nanotube array surface. It is obvious that the size of the white OCP



**Fig. 6.** Typical SEM images of the patterned OCP thin films deposited on  $\text{TiO}_2$  nanotube films with different deposition times: (a and b) 1 min; (c and d) 2 min; (e and f) 3 min; (g and h) 5 min.



**Fig. 7.** SEM image (a) of the boundary between superhydrophilic and superhydrophobic by electrochemical deposition for 5 min. EDX spectrum (b) of the superhydrophobic region.

dots is equal to that of the superhydrophilic area on template, indicating the deposited regions were only located within the superhydrophilic dots where photocatalytic degradation of PTES-SAMs was performed [37].

Fig. 6 shows the effect of the deposition time on the size and morphology of the OCP patterns. In the case of deposition for 1 min (Fig. 6a and b), no significant change in the appearance of the TiO<sub>2</sub> nanotube surface except for the darker background compared to the superhydrophobic regions. This may be explained in terms of the nucleation of pre-adsorbed Ca and P ions on the TiO<sub>2</sub> surface. As the deposition time increases to 2 min (Fig. 6c and d), it is interesting to observe that the order OCP dots have two scale sizes. The diameter in the outermost circle is ~50 μm while it decreases to ~40 μm of the innermost circle as indicated by the dotted rings. This shows the preferential growth of the quasi-vertical OCP crystals at the central region of the superhydrophilic dots. With increasing ECD time (Fig. 6e and f), both the thickness and the size increased. The spacing (~21 μm) between the edges of neighboring dots is approximately the same as that of the template (~20 μm). When ECD time was prolonged to 5 min (Fig. 6g and h), the ribbon-like OCP crystals grew so quickly that it covered some part of the adjacent superhydrophobic areas. Therefore, the edge spacing of the neighboring dots is greatly decreased to around 15 μm.

Under high magnification, ribbon-like OCP crystals with hundreds of nanometers in width and several micrometers in length, were observed at the deposition time of 5 min (indicated by arrow of a in Fig. 7a). The micro-scale polygonal pores (arrow b in Fig. 7a) consisted of TiO<sub>2</sub> nanotubes can be seen on the superhydrophobic regions. The EDX spectrum also verified that it only contains Ti and O elements within the superhydrophobic region (Fig. 7b). This result indicated the superhydrophobicity can effectively suppress

the nucleation and growth of the OCP nanocrystals due to the air trapped between the electrode/electrolyte interfaces [38]. The polygonal microstructure shape could be a result of anisotropic etching of the underlying Ti grains [39,40]. Mechanical stresses due to electrostriction and volume expansion from metal to oxide at the metal/oxide interface might also be a contributing factor [41].

The electron probe microanalyzer (EPMA) also verified the corresponding micropattern with various chemical compositions in different regions. Fig. 8 shows calcium element distribution map and the line-scan signal intensity profiles across the grid pattern by electrochemical deposition for 2 min. As can be seen in the map, large areas of ordered patterns with clear boundary were obtained from the selective deposition of OCP nanostructures in aqueous solution (Fig. 8a). The line-scan measurement was performed in a direction across the dot pattern as indicated by the pink dotted line in area-scan image. It clearly showed the element signal intensity difference between superhydrophobic and superhydrophilic areas (Fig. 8b). Oxygen, calcium and phosphorus element signal intensity increased greatly within superhydrophilic dot, while the signal intensity of Ti increased only a little after OCP deposition. This suggests that most or all of the TiO<sub>2</sub> nanotube layers in the homogeneous green grid areas corresponding to the superhydrophilic regions were covered by OCP layer, while the surrounding areas remained intact under the protection of PTES-SAMs. The slightly deviation of the detected signal intensity is due to the porous structure resulted from the spatial epitaxial growth of OCP crystals.

### 3.4. Mechanism

The mechanism of the selective OCP nucleation and growth on the cathode–electrolyte micro-contact interface is discussed

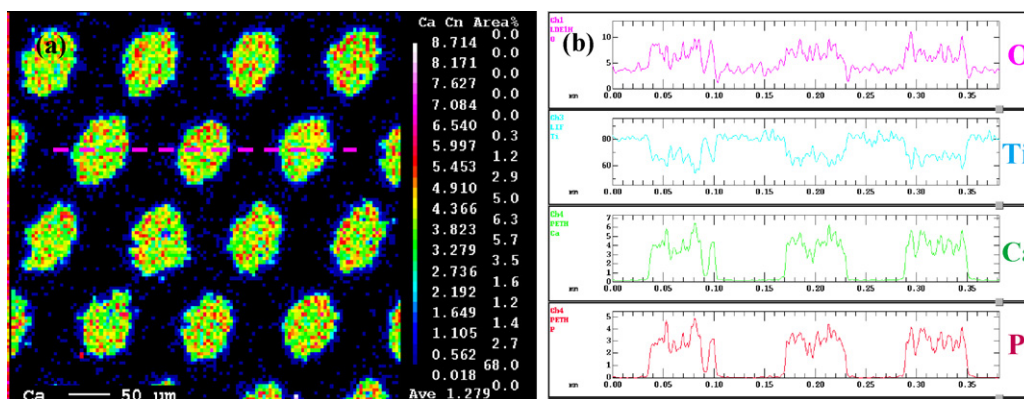


**Fig. 8.** The chemical composition map and line-scan signal intensity of the corresponding pink line along the as-prepared OCP micropattern on TiO<sub>2</sub> nanotube film by electrochemical deposition for 2 min.

here. When the ECD process is started, the current is only passing through the superhydrophilic regions due to the trapped air between electrolyte and the superhydrophobic regions. Therefore, two important products ( $\text{OH}^-$  and  $\text{H}_2$ ) generated preferentially at location of solid-liquid contact interface within the superhydrophilic region. The rise of the local pH will increase the supersaturation of CaP materials [42], and leads to the nucleation and growth of the OCP crystals on the superhydrophilic regions. The dynamic hydrogen bubbles generated and adhered at the liquid/solid interface play a vital role to the final porous nanostructure of OCP. Therefore, the patterned OCP layer possesses micro–nanodual scale structures.

One of the drawbacks of the superhydrophilic–superhydrophobic templates is the weak wettability contrast in the non-liquid solution system due to its lower surface tension. Nevertheless, the patterning effect in a water solution system is excellent, and functional materials can be easily introduced only to the superhydrophilic surface via the hydroxyl-containing groups. As a demonstration, we have used a procedure analogous to the schematic outline in Fig. 1 to assemble hydroxyapatite nanorods pattern on  $\text{TiO}_2$  nanotube array film with different liquid electrolytes by electrophoretic deposition technique (see supporting information Fig. S2).

#### 4. Conclusion

In this paper, we have demonstrated the successful application of using a superhydrophilic–superhydrophobic template to obtain position-controlled growth of ribbon-like OCP nanocrystals on  $\text{TiO}_2$  nanotube array surface. We have demonstrated the spatial epitaxial organization of the porous OCP film over large areas following prescribed wettability template. This novel micro–nanodual structure patterning strategy based on templates with extremely wetting contrast can be expanded to the selective growth of other functional materials from aqueous solution, and may contribute to the specific application of biomedical implant materials and tissue engineering scaffolds.

#### Acknowledgments

The authors thank the National Nature Science Foundation of China (20773100, 20620130427) and National Basic Research Program of China (973 Program) (2007CB935603), and R&D of Fujian and Xiamen (2007H0031, 3502Z20073004).

#### Appendix A. Supplementary data

Supplementary data associated with this article can be found, in the online version, at doi:10.1016/j.colsurfb.2009.10.023.

#### References

- [1] R. Wang, K. Hashimoto, A. Fujishima, M. Chikuni, E. Kojima, A. Kitamura, M. Shimohigoshi, T. Watanabe, *Nature* 388 (1997) 431.
- [2] K. Ichimura, S.K. Oh, M. Nakagawa, *Science* 288 (2000) 1624.
- [3] L. Feng, S.H. Li, Y.S. Li, H.J. Li, L.J. Zhang, J. Zhai, Y.L. Song, B.Q. Liu, L. Jiang, D.B. Zhu, *Adv. Mater.* 14 (2002) 1857.
- [4] X.M. Li, D. Reinhoudt, M. Crego-Calama, *Chem. Soc. Rev.* 36 (2007) 1350.
- [5] P. Roach, N.J. Shirtcliffe, M.I. Newton, *Soft Matter* 4 (2008) 224.
- [6] L. Gao, T.J. McCarthy, *Langmuir* 22 (2006) 6234.
- [7] Y. Wu, M. Kouno, N. Saito, A.F. Nae, Y. Inoue, O. Takai, *Thin Solid Films* 515 (2007) 4203.
- [8] T. Ishizaki, H. Sakurai, N. Saito, O. Takai, *Surf. Coat. Technol.* 202 (2008) 5535.
- [9] P.N. Manoudis, A. Tsakalof, I. Karapanagiotis, I. Zuburtikudis, C. Panayiotou, *Surf. Coat. Technol.* 203 (2009) 1322.
- [10] A. Kumar, H.A. Biebuyck, N.L. Abbott, G.M. Whitesides, *J. Am. Chem. Soc.* 114 (1992) 9188.
- [11] D.W. Carr, M.J. Lercel, C.S. Whelan, H.G. Craighead, K. Seshadri, D.L. Allara, *J. Vac. Sci. Technol. A* 15 (1997) 1446.
- [12] S. Xu, G.Y. Liu, *Langmuir* 13 (1997) 127.
- [13] P.L. Jae, M.S. Myung, *J. Am. Chem. Soc.* 126 (2004) 28.
- [14] B. Su, M. Li, Z.Y. Shi, Q.H. Lu, *Langmuir* 25 (2009) 3640.
- [15] C. Dorrer, J. Ruhe, *Adv. Mater.* 20 (2008) 159.
- [16] H. Liu, L. Feng, J. Zhai, L. Jiang, D.B. Zhu, *Langmuir* 20 (2004) 5659.
- [17] S.X. Hu, X.Y. Cao, Y.L. Song, C. Li, P. Xie, L. Jiang, *Chem. Commun.* 17 (2008) 2025.
- [18] F. Xia, H. Ge, Y. Hou, T.L. Sun, L. Chen, G.Z. Zhang, L. Jiang, *Adv. Mater.* 19 (2007) 2520.
- [19] K. Tadanage, J. Morinaga, A. Matsuda, T. Minami, *Chem. Mater.* 12 (2000) 590.
- [20] X.T. Zhang, M. Jin, Z.Y. Liu, D. Tryk, S. Nishimoto, T. Murakami, A. Fujishima, *J. Phys. Chem. C* 111 (2007) 14521.
- [21] X.T. Zhang, H. Kono, Z.Y. Liu, S. Nishimoto, D. Tryk, T. Murakami, H. Sakai, M. Abe, A. Fujishima, *Chem. Commun.* 46 (2007) 4949.
- [22] Y.K. Lai, C.J. Lin, H. Wang, J.Y. Huang, H.F. Zhuang, L. Sun, *Electrochem. Commun.* 10 (2008) 387.
- [23] W.E. Brown, J.P. Smith, J.R. Lehr, A.W. Frazier, *Nature* 196 (1962) 1050.
- [24] W.E. Brown, N. Eidelman, B. Tomazic, *Adv. Dent. Res.* 1 (1987) 306.
- [25] J. Lee, O. Kim, J. Jung, K. Na, P. Heo, J. Hyun, *Colloids Surf. B* 72 (2009) 173.
- [26] J.H. Lee, H.E. Kim, J.H. Im, Y.M. Bae, J.S. Choi, K.M. Huh, C.S. Lee, *Colloids Surf. B* 64 (2008) 126.
- [27] H.W. Shim, J.H. Lee, T.S. Hwang, Y.W. Rhee, Y.M. Bae, J.S. Choi, J. Han, C.S. Lee, *Biosens. Bioelectron.* 22 (2007) 3188.
- [28] V.P. Pattani, C.F. Li, T.A. Desai, T.Q. Vu, *Biomed. Microdevices* 10 (2008) 367.
- [29] Y.K. Lai, L. Sun, Y.C. Chen, H.F. Zhuang, C.J. Lin, J.W. Chin, *J. Electrochem. Soc.* 153 (2006) D123.
- [30] Y.K. Lai, C.J. Lin, J.Y. Huang, H.F. Zhuang, L. Sun, T. Nguyen, *Langmuir* 24 (2008) 3867.
- [31] H. Wang, C.J. Lin, R. Hu, F. Zhang, L.W. Lin, *J. Biomed. Mater. Res. A* 87 (2008) 698.
- [32] E. Balaur, J.M. Macak, H. Tsuchiya, P. Schmuki, *J. Mater. Chem.* 15 (2005) 4488.
- [33] K. Das, A. Bandyopadhyay, S. Bose, *J. Am. Ceram. Soc.* 91 (2008) 2808.
- [34] Y.K. Lai, H.F. Zhuang, L. Sun, Z. Chen, C.J. Lin, *Electrochim. Acta* 54 (2009) 6536.
- [35] Y.K. Lai, J.Y. Huang, J.J. Gong, Y.X. Huang, C.L. Wang, Z. Chen, C.J. Lin, *J. Electrochem. Soc.* 156 (2009) D480.
- [36] Y. Zhu, M.H. Shi, X.D. Wu, S.R. Yang, *J. Colloid Interf. Sci.* 315 (2007) 580.
- [37] J.P. Lee, H.K. Kim, C.R. Park, G. Park, H.T. Kwak, S.M. Koo, M.M. Sung, *J. Phys. Chem. B* 107 (2003) 8997.
- [38] Y.K. Lai, X.F. Gao, H.F. Zhuang, J.Y. Huang, C.J. Lin, L. Jiang, *Adv. Mater.* 21 (2009) 3799.
- [39] G.A. Crawford, N. Chawla, *Acta Mater.* 57 (2009) 854.
- [40] Y.K. Lai, Z.Q. Lin, J.Y. Huang, L. Sun, Z. Chen, C.J. Lin, *New J. Chem.* (2009), doi:10.1039/b9nj00325h.
- [41] K. Yasuda, J.M. Macak, S. Berger, A. Ghicov, P. Schmuki, *J. Electrochem. Soc.* 154 (2007) C472.
- [42] R. Hu, C.J. Lin, H.A. Shi, *J. Biomed. Mater. Res. A* 80 (2007) 687.